48th AIAA/ASME/SAE/ASEE Joint Propulsion Conference & Exhibit
30 July - 01 August 2012, Atlanta, Georgia

AIAA 2012-3961

Visualization of the Liquid Layer Combustion of Paraffin Fuel for Hybrid Rocket Applications

Ashley Chandler[1], Elizabeth Jens[2], Brian J. Cantwell[3], and G. Scott Hubbard[4]
Stanford University, Stanford, CA, 94305

The adoption of the hybrid design for large rocket motors has been hindered by the slow regression rate associated with classical hybrid fuels and consequentially, the requirement for complex, multiport fuel grains. High regression rate hybrid fuels (e.g. paraffin) enable simple, single port hybrid propulsion systems for a variety of applications including launch vehicles, solar system exploration and space tourism. The mechanism responsible for the increased regression rate of these fuels is still not fully understood. Therefore, an apparatus has been constructed at Stanford University to visualize the combustion of high regression rate hybrid fuels in order to compare it with the predicted mechanism. It consists of a flow conditioning system and combustion chamber with three windows. The combustion is captured using two high-speed video cameras for both top and side views. The behavior of paraffin-based fuel is compared to that of classical hybrid fuels. Both the experimental design and results of seven tests with five hybrid fuels and gaseous oxygen are presented. Results of two additional tests are included for increased detail. The results are consistent with the droplet entrainment mechanism generally used to explain the high regression rates exhibited by paraffin-based fuels.

Nomenclature

O/F = oxidizer to fuel ratio

I. Introduction

HYBRID rockets typically consist of a liquid oxidizer and solid fuel. They embody many of the key benefits of each of their parent systems while eliminating some of the main drawbacks. Some advantages of hybrid rockets as compared to solid rockets include: increased performance, safety, ability to throttle and tolerance to debonding/cracks. In comparison to liquids, hybrids are less complex, easier to throttle, and safer. The fuel regression rate is nearly independent of chamber pressure, allowing increased design flexibility. However, classical hybrid rockets have been plagued by the slow solid fuel regression rate of polymeric fuels. This most often requires the use of complex, multiport fuel grains in order to obtain the thrust rates required by typical applications. The disadvantages associated with multi-port hybrid fuel grains overpower many of the advantages of hybrid rockets.

The discovery of liquefying hybrid fuels, such as paraffin, has revitalized research in hybrid rockets over the past decade. The fast burning rate enjoyed by paraffin-based hybrid fuels makes them excellent candidates for a variety of applications including: launch vehicles, solar system exploration and space tourism. However, the mechanism responsible for this increased regression rate is not fully understood.

---

[1] PhD Candidate, Department of Aeronautics and Astronautics, 496 Lomita Mall, Durand Building Room 051, Stanford, CA 94305, and AIAA Member.
[2] PhD Candidate, Department of Aeronautics and Astronautics, 496 Lomita Mall, Durand Building Room 051, Stanford, CA 94305, and AIAA Member.
[3] Edward C. Wells Professor, Department of Aeronautics and Astronautics, 496 Lomita Mall, Durand Building Room 379, Stanford, CA 94305, and AIAA Fellow.
[4] Professor - Consulting, Department of Aeronautics and Astronautics, 496 Lomita Mall, Durand Building Room 363, Stanford, CA 94305, and AIAA Fellow.

Ref. 1 proposes that these fuels produce a thin liquid layer on the surface when they burn. The liquid layer has low surface tension and viscosity and therefore is unstable under the shear force from the vaporized oxidizer flow. This leads to the formation of roll waves and the entrainment of droplets into the gas stream. The entrainment mechanism effectively acts like a spray injection system distributed along the fuel port, greatly increasing the mass transfer rate of the fuel and hence the fuel regression rate (by 3-4 times that of conventional hybrid fuels). Ref. 2 describes this proposed entrainment process in detail.

II. Motivations for an Experiment

The goal of this experiment is to support improved combustion models and simulations of these fuels by observing the mechanism responsible for the increased regression rate. The experiment is designed to provide information to determine if the high regression rate of liquefying fuels is due to the liquid layer instability leading to roll waves and droplet entrainment described in Ref. 2. It will also provide a test bed for many future experiments. The flow system was designed to be very flexible in order to adapt to ongoing results. Some of the original motivations include determining the general size, shape and speed of the entrained fuel in the oxidizer flow over a range of pressures from one atmosphere to a maximum working pressure of 1.72 MPa, which is well above the supercritical pressure for paraffin. Refs. 3 and 4 have made previous optical visualizations of this process at atmospheric pressure. The atmospheric pressure tests presented here can be compared with the results of these previous investigations.

III. Experimental Set Up

The visualization facility is presented in Figure 1. It is made up of three main components: the feed system, flow conditioning system and the combustion chamber. The feed system delivers gaseous oxygen and nitrogen to the combustion chamber from the adjoining room. The oxygen cylinders are kept away from the combustion chamber for safety purposes. The oxidizer flow can be controlled with a metering valve in the line. The nitrogen is used to quench the flame and purge the system of oxidizer and combustion products. A full explanation of the valves and complexities of this system is left to Ref. 5. The main goal of the flow conditioning system is to produce a uniform and predictable flow at the inlet to the combustion chamber. It is essentially a low speed wind tunnel with oxygen as the working gas. The final component is the combustion chamber. It is brass with three rectangular windows, on both sides and the top, to allow visual access to the combustion chamber from multiple vantage points and a variety of lighting options. A small slab of paraffin is fixed to a cantilevered support. This design was selected to insure that the combustion does not contact the walls and windows of the device. The mass flux of the apparatus was designed to overlap with experiments previously conducted at Stanford University. More detail on the subsystems is given in the following paragraphs. If more information is desired, a full description of the experimental set up is provided in Ref. 5.

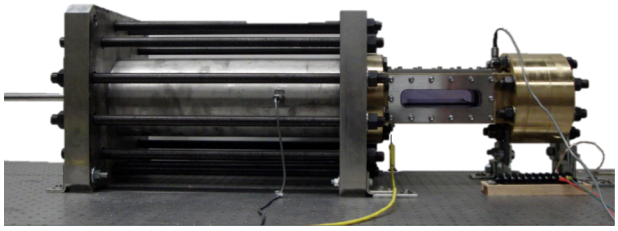

Figure 1. Experimental Set Up. *The flow conditioning system and combustion chamber. Flow is from left to right.*

A. Flow Conditioning System

A flow conditioning system is employed in order to create a uniform and predictable velocity profile at the inlet of the test section. The design of the test section, while optimal for some parameters, does not make it simple to predict how much of the oxidizer is able to react with the fuel. Therefore, it is desirable to get a more accurate picture of the flow over the solid fuel. A diffuser, three-screen settling chamber and contraction are used to increase the uniformity of the oxidizer flow before entering the test section. The flow conditioning system was designed using rules developed for small, low speed wind tunnels.[6] In order to confirm that the system behaved as predicted, a mock up

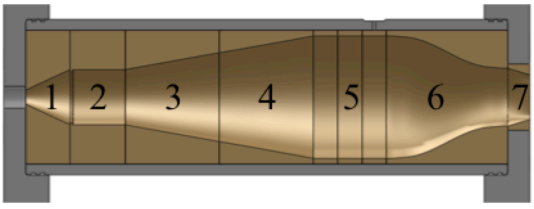

Figure 2. Flow Conditioning System. *A CAD drawing of the flow conditioning system. The inserts include: 1. Inlet, 2. Reservoir, 3-4. Wide angle diffuser, 5. Settling chamber, 6. Contraction, 7. Circle to square transition. Flow is from left to right. Screens are located between each insert.*

of the diffuser and settling chamber were built and tested using a water channel in the Fluid Mechanics Laboratory at NASA Ames Research Center. No large-scale separation in the diffuser was observed during the water channel tests and the resulting flow at the outlet was fairly uniform. Any significant lingering non-uniformity at the end of the settling chamber will be further reduced by the contraction. Full results of these tests are presented in Ref. 5.

Flow enters the conditioning system from the left and expands rapidly in the inlet (component 1.) A flow trip is present at the upstream end of the reservoir (component 2) to encourage transition to turbulent flow. Components 3 and 4 make up a wide-angle diffuser (20 degrees.) A three screen settling chamber is used to reduce any variations in the stream wise direction and is indicated by 5 in Figure 2. There is a pressure tap in the last insert of the settling chamber. A contraction (with an area ratio of 4.41) is used to reduce any lingering non-uniformities. Component 7 transitions the flow from the circularly symmetric flow conditioning system to the combustion chamber, which is a square with filleted corners.

B. Combustion Chamber

The combustion chamber is made of a readily machinable brass alloy, brass 360, for oxidizer compatibility. Brass has favorable thermal conduction behavior as well. The combustion chamber is shown in Figure 3. The inner dimensions of the combustion chamber are 5.08 cm by 5.08 cm square with filleted edges (0.635 cm radius.) It has three rectangular windows, on both sides and the top, to allow visual access to the combustion chamber from multiple vantage points as well as a variety of lighting options. The windows allow a view into the combustion chamber that is 2.8 cm high by 17.4 cm long on each of the three sides.

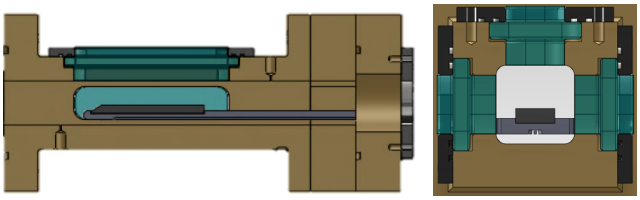

(a) (b)

Figure 3. Combustion Chamber. *CAD drawings of the combustion chamber. (a) A centerline cut-through. Flow is from left to right. (b) A cut-through about one third of the way along the combustion chamber. Flow is into the page.*

The windows are made of polycarbonate for low cost. This places an upper limit on the burn time such that the windows do not overheat. This limit is mainly set by the size of the fuel grain the system can accommodate while insuring the combustion process does not interact with the windows.

Both pressure and temperature measurements are taken inside the combustion chamber. The taps for each of these instruments are visible in Figure 3 a. A 1/16th inch K-type thermocouple is installed at the bottom of the combustion chamber, upstream from the combustion. The probe is inserted such that the sheath is flush with the base of the combustion chamber and the exposed junction extends upward for several millimeters. This gives us a reference temperature for the flow. The measurement error associated with the thermocouple is ±1.1 C. The pressure is measured with a Measurement Specialties US300 type transducer. It is installed downstream of the combustion, on top of the combustion chamber. The diaphragm is coated with Krytox, an oxygen compatible lubricant, to protect it from the combustion gases. The error associated with these measurements is ±3100 Pa.

Values for the important parameters in the combustion chamber are presented in Table 1. The oxidizer mass flow is taken to be the maximum currently achievable and the other values are calculated. The cold values are representative of a cold flow (no combustion) and use data for Oxygen from NIST.[7] The hot values are calculated at the adiabatic flame temperature using Chemical Equilibrium with Applications.[8] This calculation assumes stoichiometric combustion at atmospheric pressure with an area ratio of one.

Parameter	Cold Value	Hot Value
Oxidizer Mass Flow [kg/s]	0.07	
Temperature [K]	293	3102
Density [kg/m^3]	1.33	0.094
Velocity [m/s]	28	30-110
Ratio of Specific Heats	1.40	1.23
Viscosity [Pa s]	2.0 x 10^{-5}	1.0 x 10^{-4}
Reynolds Number [cm^{-1}]	18600	3700
Prandtl Number*	0.71	0.65

Table 1. Combustion Chamber Parameters. *The hot values were calculated assuming a stoichiometric reaction at room temperature and atmospheric pressure and with an area ratio of one. *The hot case assumes frozen reaction.*

C. Fuel, Support, and Ignition

The fuel grains are each approximately 2.5 by 1 by 12.7 cm with a chamfered leading edge. The paraffin based fuel grains were cast in a silicone mold and left to cool in a vacuum-sealed bag. This minimized the number of bubbles in the wax and helped remove the large bubble that would often form at the aft end of the fuel grain (top of the mold.) The Hydroxyl Terminated Polybutadiene (HTPB) fuel sample was cast in a large pan and cut to size. The top surface of the HTPB was smooth, however, the need to cut the bottom and one side for each fuel grain, left those surfaces somewhat rougher. The chamfer for the HTPB was cut from the bottom such that the entire top surface would be smooth. Chemicals to form the HTPB were ordered from Rocket Motor Components, Inc. The High Density Polyethylene (HDPE) fuel grains were ordered from McMaster-Carr. They were machined and sanded to the appropriate dimensions.

In each case, the fuel is epoxied to a copper cantilevered support. A 26-gauge nichrome wire is placed across the fuel grain near the edge of the chamfer. It is coated with epoxy to ignite the fuel. The requirement that insulation remain between the lead wires and the holes on the diving board sets a limit on how closely the igniter wire can be positioned to the surface of the fuel grain. Sacrificial stranded copper lead wires are fed through holes on either side of the fuel grain and run along a Y-shaped groove in the base of the copper support and out the aft end of the combustion chamber. High temperature G10 garolite was originally used for the fuel support. While commonly used as an insulator, the fiberglass/epoxy composite material burns in pure oxygen. After about a second, the fuel support began burning and seeding the flow, changing the boundary layer significantly. There was one instance where this was actually beneficial and will be reported in the results section.

Figure 4. Fuel, Support and Ignition. *The fuel grain is epoxied to the copper support. A nichrome wire is placed just behind the chamfer at the fore end. It is coated with epoxy to ignite the fuel. Lead wires run under the support and out the aft end of the combustion chamber.*

D. Camera

The combustion of each of the hybrid fuels will be captured optically with a Casio Exilim EX-F1, capable of 1200 frames per second. The resolution of the camera decreases with increased frame rate. However, instead of capturing the same area with a reduced number of pixels, the available area is reduced at high speeds. At 1200 fps, the visible area is a long, slender rectangle (336 x 96 pixels.) The rectangular shape of the windows complements the available area of the camera at these high speeds.

IV. Tests

The results from tests with five fuels will be discussed. Three variants of paraffin fuel are included: plain paraffin ($C_{32}H_{66}$), the same type of paraffin with a black dye added (0.5% by mass) and SP1X-01 (a blackened paraffin with strength and regression rate additives.) The latter has the same regression rate behavior as SP1A presented in Ref. 9. Two classical fuels were tested for comparison. High density polyethylene (HDPE) is a classical fuel that is expected to form a liquid layer on the surface. However, the liquid layer is expected to be too viscous to support substantial entrainment. The other classical fuel being tested (HTPB) is not expected to form a liquid layer nor entrain. It will be the main control case to which the paraffin runs can be compared. A summary of these tests is presented in Table 2.

Data from two additional tests: one with blackened paraffin and the other with HTPB (the control) are included to complement these results. The main difference between these tests and the previous ones was a physical change in camera location. The high speed mode on the camera fixes the number of pixels available, therefore, this zoomed in view enables higher resolution images. The side view camera was moved from just over 3 m away to 0.82 m away. The top view camera was 1.02 m from the test section for both tests. These tests were conducted to get a better picture of the liquid layer. A summary of these tests is given in Table 3.

Finally, two previous tests with classical hybrid fuels will be included to clarify several results. These tests were conducted using a different material for the fuel support. As described earlier, the garolite support had several problems, including that it burns in pure oxygen. However, that combustion actually illuminated the fuel surface and allowed the observation of a flowing liquid layer in the HDPE case. An HTPB example will be included during the

		Paraffin-based fuels			Classical fuels	
		Paraffin	**Blackened paraffin**	**SP1X**	**HDPE**	**Blackened HTPB**
Test date		23 May 2012	23 May 2012	22 May 2012	23 May 2012	23 May 2012
Average Oxidizer Mass Flux (g/cm^2s)		3.19	2.61	3.31	2.88	2.94
Programmed burn time (s)		2.5	2.5	2.5	3	3
Approx. actual burn time (s)		3.5	3.5	3.4	4.7	4.1
Burned mass (g)		6.7	6.0	5.9	1.7	2.8
Average O/F		32	29	36	152	82
Side view camera settings	**Frame rate (frames per s)**	1200	1200	1200	1200	1200
	Fstop	4.6	4.6	4.6	4.6	4.6
	Shutter speed (s)	1/32,000	1/32,000	1/32,000	1/32,000	1/32,000
Top view camera settings	**Frame rate (frames per s)**	1200	1200	240 *	1200	1200
	Fstop	4.4	3.5	4.9	3.5	3.5
	Shutter speed (s)	1/32,000	1/32,000	1/32,000	1/32,000	1/32,000

Table 2. Test Summary. *One test with each fuel is presented in this table and will be further discussed in this section. All tests were conducted at atmospheric pressure. *Different camera used for this test (Casio EX-FH25)*

discussion of flame vortex roll up. In this case, it was the minimal level of windows damage that led to its inclusion. As described earlier, the system was designed to minimize the interaction of the combustion with the windows. However, in the early phases of this test program, some damage was incurred. It was mainly due to the slow, initial purge and one test with an oversized HTPB fuel grain.

Each test was run using the same LabVIEW program to control the valves and acquire data. The oxidizer flow was initiated first, and then voltage was applied to the igniter. Combustion was sustained for the duration of the oxidizer flow. The nitrogen purge is started prior to shutting off the oxygen in order to minimize the possibility of back flow through the system. It typically takes 1-2 seconds for the flame to be fully quenched while the remainder of the oxygen is flushed from the system. The set up, test, then disassembly of the system takes 1-2 hours per test.

A differential pressure transducer is used to measure the average oxidizer mass flux across a venturi in the oxygen line. This can be altered using a manual metering valve in the oxygen line. Currently, two T-sized cylinders supply gaseous oxygen using Victor SR4J regulators. Unfortunately, at the highest mass flow rates the high-pressure regulators on the DOT oxygen cylinders become the limiting orifice in the oxidizer flow. Therefore the pressure drop in the oxygen cylinders causes a small drop in mass flow during a run. This will be changed in the future to enable higher mass fluxes.

Two burn times are reported in the tables. The first is the programmed burn time. This is the length of time for which the main oxidizer valve is programed to be open. An additional tenth of a second is added on to prevent back flow of the gases. However, the system takes a reasonably long period of time to clear. The actual burn time is approximated from the high-speed video. The number of frames from the time the igniter lights to when the purge is clearly visible is reported.

		Blackened Paraffin	**HTPB**
Test date		25 May 2012	25 May 2012
Average Oxidizer Mass Flux (g/cm^2s)		2.69	2.58
Programmed burn time (s)		2	2
Approx. actual burn time (s)		3.4	3.5
Burned mass (g)		5.1	1.6
Average O/F		34	107
Side view camera settings	**Frame rate (frames per s)**	1200	1200
	Fstop	4.6	3.6
	Shutter speed (s)	1/32,000	1/32,000
Top view camera settings	**Frame rate (frames per s)**	1200	1200
	Fstop	3.6	4.6
	Shutter speed (s)	1/32,000	1/32,000

Table 3. Zoomed in Test Summary. *The cameras for each of these tests were zoomed in considerably from the previous tests to capture more detail. All tests were conducted at atmospheric pressure.*

Since each frame is only 1/1200th of a second, this value should be fairly accurate.

Each fuel grain is weighed before it is attached to the fuel support. The burned fuel mass is calculated by subtracting the mass of fuel left after the burn from its original mass. The fuel grains are attached to the support with epoxy. It is not difficult to remove most of the epoxy from the paraffin and HDPE cases; however, it is quite hard to ensure that it is removed from the HTPB.

V. Results

Results from the seven tests are presented. The images presented in the following sections are stills from the high-speed video taken during each of the tests. The results are not presented in the order the tests were conducted. An over all discussion of the results from all of the tests is included in the next section.

A. Paraffin

This sample was plain $C_{32}H_{66}$, also called FR5560 as ordered from the Candlewic Company. The test was successfully run in the morning of 23 May 2012. The flame is thicker at the fore end of the grain while the flame is developing, however, it evens out to a more uniform flame as the run progresses. The combustion becomes more stable at the same time. Droplets are visible above the flame. Figure 5 shows that the flame sheet appears to be drawn out into highly elongated filaments similar to the mixing in a cold, variable density, channel flow visualized computationally by Haapanen[10].

Figure 5. Paraffin Flame. *The flame appears to be made up of elongated filaments.*

A thin coat of wax was left on the fuel support and some accumulated in the nozzle section as well. It appears that the melted layer is pushed off the back of the fuel grain and continues flowing along the diving board. The layer on the fuel support was removed intact and was measured to be approximately 0.3 mm thick. The layer reveals an initial outward motion of the flow and then a contraction at the end of the test section. It finally expands again as it flows past the T in the fuel support. Both veins are ripples are visible in the layer.

B. Blackened Paraffin

This test utilizes the same paraffin wax as discussed in the last section with the addition of black dye. The dye limits radiation penetration into the solid fuel grain. The fuel ignited without incidence and flame vortex rolling was observed at the aft end of the fuel grain. The flame takes 0.34 seconds to reach the end of the fuel grain. During the early part of the burn, there is a zone glowing red outside the brightest part of the flame. The red zone fades out after 0.8 seconds and the flow becomes its characteristic white and blue color with filament-like structures (Figure 6.)

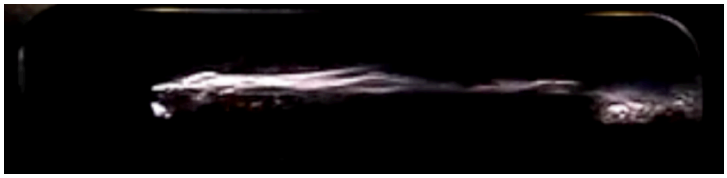

Figure 6. Blackened Paraffin Flame. *The flame appears to be made up of elongated structures.*

Droplets are visible throughout the burn. Figure 7 is a composite image of two consecutive frames, which shows the progression of a single droplet (circled in red.) The top view camera, Figure 8, shows the common paths taken by the droplets. A single droplet is shown moving between three consecutive frames (again circled in red.) However, only the brightest droplets can be seen with these camera settings.

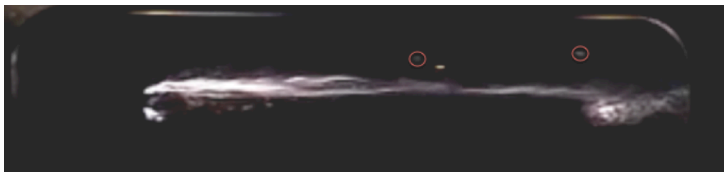

Figure 7. Droplet in Blackened Paraffin. *A droplet moving between two consecutive frames.*

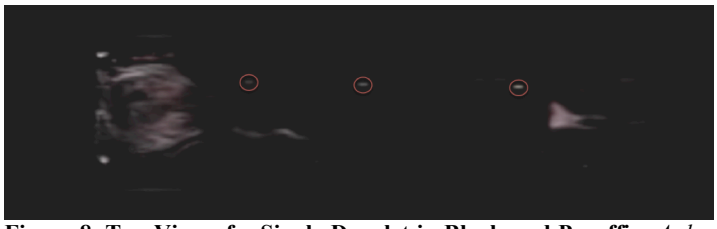

Figure 8. Top View of a Single Droplet in Blackened Paraffin. *A droplet moving between three consecutive frames as captured from above the combustion chamber.*

It was difficult to determine where the liquid layer was in these images. This was one

of the driving factors for including the second set of tests. The video of this test was re-examined after conducting the zoomed in tests. Similar features, including roll waves can be observed in this video. However, the detail in which they can be seen in the zoomed-in case cannot be matched by these images. The roll waves from this test are presented in Figure 9.

Figure 9. Roll Wave in Blackened Paraffin. *Instabilities in the liquid layer can be observed in this test.*

C. SP1X-01

SP1X is based off the plain paraffin reported earlier, however it has additives that alter the strength and regression rate of the material. This fuel can most closely be compared to SP1A and shares the same regression rate law.

The flame takes approximately 0.42 s to propagate to the end of the fuel grain, with a tenth of a second just for the flame to extend beyond the ignition zone. This is somewhat slower than the case without additives. The portion of the boundary layer illuminated by the flame fluctuates between the typical thin layer and a more full layer, which is approximately 3-4 times the size due to combustion instability. There are interesting filament-like features during this run. Figure 10 shows this instability through two still images that are seven frames apart.

This fuel produced droplets above the flame as in the previous cases. However, not in overwhelming amounts.

The paraffin-based fuel melted slightly in the recess of the diving board. The timing of the melting is unknown. It is reasonable to assume that at least some of this occurred after the burn while the copper was still warm. The final shape of the fuel grain has elevated ridges near the two sides. The area under the igniter is also raised. These ridges vary in height somewhat, but are approximately 6 mm tall, slightly taller in the back. The area under the igniter is raised to 7.5 mm. and the center of the fuel is about 5.2 mm. There is a slight asymmetry in the flow by the path chosen by the liquid layer. The melt layer removed from the fuel support was approximately 0.2 mm thick and 0.2 grams of wax was removed from the nozzle section.

Figure 10. SP1X Combustion Instability. *The top and bottom images are seven frames apart.*

D. HDPE

High-density polyethylene is expected to form a liquid layer, however the viscosity of the liquid layer is much higher than paraffin and it is not expected to produce significant droplet entrainment. This is supported by the strongly decreased burned mass compared to the paraffin cases (Table 2.) However, droplets are visible above the flame throughout the burn, see Figures 11 and 12.

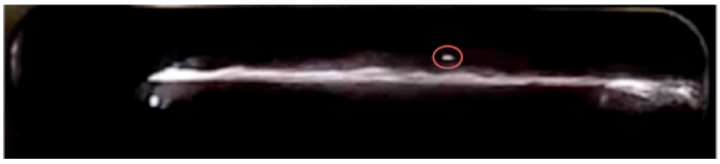

Figure 11. HDPE Droplets. *One of the droplets from the HDPE test.*

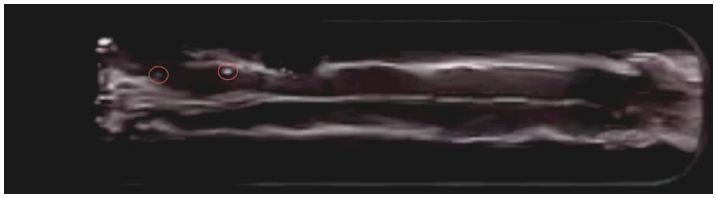

Figure 12. HDPE Top View Droplet. *This is a composite image of two consecutive frames. The same droplet is circled in each frame.*

Evidence of a small amount of burning along the sides of the fuel grain is visible upon examination of the grain after the burn. Darkened spots are present along the sides, especially towards the back. The fuel grain bowed upwards substantially, indicating either the force of the oxidizer flow, heat from the combustion/copper fuel support or some combination of both affected the material. After the burn, parallel ridges are visible running along the sides of the fuel grain. The path behind the fuel grain is outlined on the copper diving board. It appeared to be mainly

combustion products and caused some discoloration of the fuel support.

The flame appears quite different from the paraffin cases. It takes nearly a full second (0.98 s) for the flame to reach the end of the fuel grain. This is more than double the time the paraffin-based fuels take to propagate. The flame is fairly thin throughout the length of the burn. The flame sheet rolls at the end of the fuel grain as in the previous cases. This is especially noticeable at the beginning of the run. Droplets are formed and escape during this period and through out the burn. They tend to follow similar paths. The top view camera only revealed the brightest features in the combustion process. At this exposure level, droplets can also be seen from the top view camera. Several of the droplets originate near the igniter wires, leading to concern that some droplets may actually be burning pieces of insulation or copper lead wires. Great care was taken to minimize this possibility, however, it is worth noting.

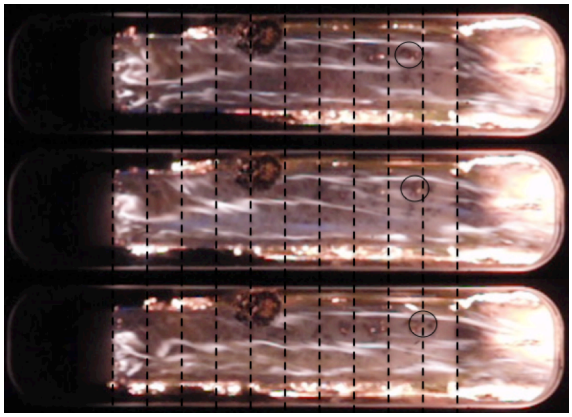

Figure 13. Top View of HDPE. *A single feature in the HDPE liquid layer is tracked through three frames which are 0.2 seconds apart (circles). The dashed lines are given for reference. This test was conducted using the G10 fuel support. (See Ref. 5 for more information.) A burned spot on the windows can be seen in the upper left portion of each frame.*

The surface of the fuel grain was not bright enough to view the motion of the liquid layer during this run. Therefore, an image from a previous test is included to illustrate this motion. The burning of the G10 fuel support illuminated the surface of the HDPE fuel grain and features in it could be seen moving in what appeared to be a relatively constant, laminar flow. Based on this movement one may estimate a liquid layer velocity of 1.25 mm/s. The set up for this test is presented in Ref. 5.

E. Blackened HTPB

Blackener was added to the HTPB mixture to minimize radiation penetration (as with the paraffin case.) This resulted in a dark grey colored fuel grain. The three sides of the fuel exposed to the flow got significantly blacker after the run. The bottom of the fuel grain was still more nearly grey after it was removed from the diving board. A trail behind the fuel grain, along the fuel support appeared after the run. It had a dense, powdery consistency.

The high-speed video is slightly over exposed during this run. It appears that the modest temperature difference between the paraffin and HTPB has a substantial affect on the brightness. There is consistently flow structure at the downstream end of the flame. This is displayed in Figure 14, circled in blue.

Only a handful of droplets can be seen over the course of the burn. It should be noted that it is possible that what appear to be droplets (illuminated elliptical blobs) could actually be pieces of the igniter burning. Even if the droplets come from the fuel, there are not enough to significantly affect the mass transfer as expected. The top view camera gives depth to the side view images. The flow seems fairly uniform, with some inward rotation. This is could be caused by vortices wrapping over the edges of the copper fuel support. There is only a 3 mm gap between the edge of the fuel support and the window to minimize this possibility.

Figure 14. HTPB. *The flame from the HTPB run. Flow structure is clearly visible at the aft end. The flame is much brighter than the previous*

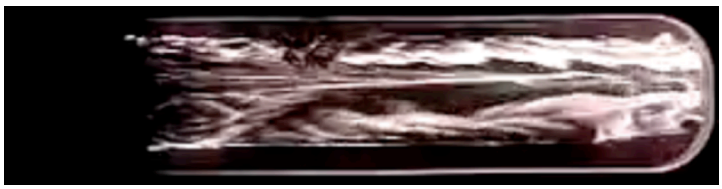

Figure 15. Top View of HTPB. *The top view from this test. As in the HDPE case, the dark mark on the top of this image is preexisting window damage.*

F. Blackened Paraffin, Zoomed in View

A much more detailed picture of the combustion can be obtained by focusing in on a smaller area of the fuel grain. The limited number of pixels can be used to better define the structure in the smaller area. The camera was lined up such that the front edge of the fuel grain was visible (see the far left of Figure 16.) The igniters burned a little during this test (as in the previous cases.) This can be seen in the bottom near the left side of the images.

The liquid layer is clearly visible throughout the run, (especially in Figure 17, where it is labeled.) The

instabilities in the liquid layer are apparent throughout the run. Roll waves are created and bursts of droplets are entrained into the flow. The waves form periodically: about 70 times over the 3.4 second burn time or at about 20 Hz. It would be interesting to see how this changes with mass flux, pressure, etc.

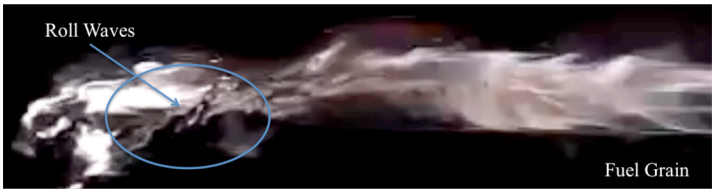

Figure 16. Roll Waves in Blackened Paraffin. *The instability in the liquid layer is visible in the form of a large wave (circled in blue) near the fore end of the fuel grain.*

As in the previous cases, droplets can be seen above the flame zone, however, it appears that many more droplets are being entrained into the flow at or below the flame as a result of the roll waves. Figure 17 shows tens of droplets being released somewhat explosively into the flow very near the fuel grain. Over a typical burn time, something on the order of several hundred drops were visible above the flame level. This mechanism appears to be capable of entraining on the order of thousands of drops in the flow and is most likely the main cause of the regression rate increase. The droplets nearest the flame would be most likely to fully combust as well. This also explains the low regression rate of HDPE even though some droplets were visible above the flame during that run.

Figure 17. Droplets in Blackened Paraffin. *Tens of droplets being released into the flow very near the solid fuel surface. The liquid layer, which extends the length of the image, is illuminated by the nearby flame zone.*

G. HTPB, Zoomed in View

HTPB is run under the same conditions in order to confirm that the combustion mechanism observed in the zoomed in paraffin run was not a result of the experimental set up. HTPB is not expected to produce roll waves nor entrain. This test confirmed that behavior. The flame is slightly overexposed, but does not show any signs of a liquid layer nor instabilities. Figure 18 is a typical image from this run. The operating conditions are given in Table 3. The igniter can be see burning in the bottom left hand side of the image, below the main flame region.

Figure 18. Zoomed in HTPB. *No liquid layer was observed in these tests.*

VI. Discussion

The results of these tests are consistent with the roll wave and entrainment mechanism described in Ref. 2. The start up and shut down periods also gave interesting insight into the combustion process. Just as the flame reaches the end of the fuel grain, vortex flame roll up is observed. This phenomenon is typically predicted to occur in hybrid combustion and will be discussed in the next section. At the end of each run, the oxygen is purged from the system with a much lower flow rate of gaseous nitrogen. The low flow rate allows the combustion to continue for an additional 1-2 seconds; however it changes completely. What is being termed "flame bursting" occurs during this time. Small jets occur on the exposed fuel surfaces. This is discussed further in Section B.

A. Vortex Flame Roll Up

Diffusive transport processes play a large role in determining the flame location in hybrid combustion. The flame occurs where there exists a combustible O/F and instability of the flame sheet can lead to vortex roll-up. The backward facing step at the aft end of the fuel grain creates a sharp cut off in available fuel and creates a region of recirculation in the flow.

Vortex flame roll up was visible in all of the fuels, however, the especially bright flame produced by the HTPB allowed the visualization of flame roll up with both the copper and G10 fuel support as shown in Figure 19.

As the flame develops, the area behind the fuel grain gets too bright to monitor details of the flow structure. Therefore, the roll up can only be seen at the very beginning of the run. The best images of this phenomenon are actually from the earlier test (HTPB with the G10 diving board) because some damage was done to the bottom part of the windows over the course of the test series, which obscures the detail below the level of the fuel grain. Figure 19 shows the flame roll up in the early runs and Figure 20 shows it in the test reported here. It is expected that this will again become more apparent upon the installation of new windows, which is planned for Summer 2012.

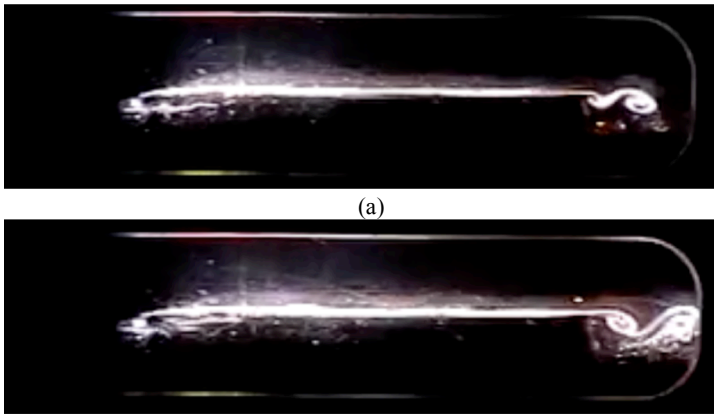

(a)

(b)

Figure 19. Vortex Flame Roll Up. *The flame rolling at the end of the fuel grain. Both images are from a previous test with HTPB/GOx using the G10 fuel support. (Test 8 on 5 May 2012 in Ref. 5)*

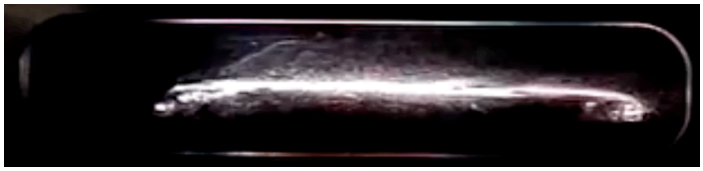

Figure 20. Vortex Flame Roll Up in HTPB. *The flame rolling at the end of the fuel grain.*

B. Flame Bursting

The other interesting feature happens at the end of the run. The mass flux is decreased substantially as the flow shifts to the gaseous N_2 line. The N_2 line is smaller and runs at a lower pressure than the O_2 line. As reported earlier, it takes several seconds to completely clear the combustion chamber of the remaining oxygen. Thus the terminal phase of combustion takes place at very low flux.

Localized reactions, evidenced by bursts of flame projecting nearly normal to the main flame sheet, continue during this process. This can be seen at the front of the blackened paraffin in Figure 21a and along both the top and the sides in the blackened HTPB (Figure 21b.) The flame bursting is immediately evident upon the beginning of the purge in both cases. It appears that these events arise from a fuel-surface-flame interaction process that occurs constantly throughout the burn, but is obscured at the higher flow speeds during the main combustion period. The lower oxidizer mass flux gives insight into what may be an important aspect of the underlying fuel mass transfer process.

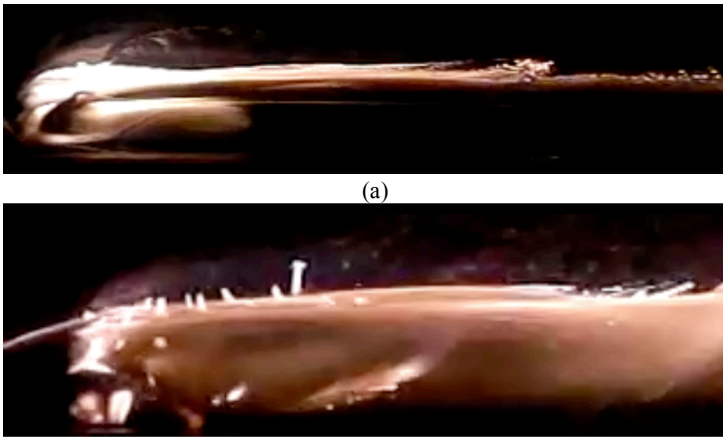

(a)

(b)

Figure 21. Low Mass Flux Flame Bursting. *Localized reactions visible at the end of the burn. (a) Zoomed in blackened paraffin. (b) Zoomed in HTPB.*

VII. Conclusion

The liquid layer combustion of paraffin-based fuels has been captured using high-speed video. Both the high regression rate (paraffin-based) and classical fuels behave as predicted. A mechanism, consistent with that predicted by Ref. 2 was observed in the tests of paraffin-based fuels. These fuels were shown to have a highly unstable liquid layer under the oxidizer flow. Periodic formation of roll waves and droplet entrainment was observed. A stable liquid layer was observed in HDPE. HTPB did not produce the roll waves or droplet entrainment observed in the paraffin-based fuels as expected. Initial observations of flame bursting events will be extended in further studies that will include the effects of pressure on the fuel entrainment and combustion process.

Acknowledgments

The authors would like to thank the Jet Propulsion Laboratory's Strategic Research University Partnership (SURP) program and Stanford University for financial support of this project. They would also like to thank Greg Zilliac and Arif Karabeyoglu for helpful discussions throughout the development of this experiment.

References

[1] Karabeyoglu, M. A., Altman, D., and Cantwell, B. J. *Combustion of Liquefying Hybrid Propellants: Part 1, General Theory.* J Prop Power Vol. 18, No. 3, May–June 2002.

[2] Karabeyoglu, M.A., Cantwell, B.J., and Altman, D. *Development and Testing of Paraffin-Based Hybrid Rocket fuels.* AIAA 2001-4503. 37th AIAA/ASME/SAE/ASEE Joint Propulsion Conference and Exhibit July 8-11,2001/Salt Lake City, Utah.

[3] Nakagawa, I., Hikone, S. and Suzuki, T. *A Study on the Regression Rate of Paraffin-based Hybrid Rocket Fuels* 45th AIAA/ASME/SAE/ASEE Joint Propulsion Conference & Exhibit 2 - 5 August 2009, Denver, Colorado, USA. AIAA-2009-4935.

[4] Pelletier, N., *Etude des Phenomenes de Combustion dans un Propulseur Hybride Modelisation et Analyse Experimentale de la Regression des Combustibles Liquefiables*, Ph.D. thesis, Universite de Toulouse, Toulouse, France, 2009.

[5] Chandler, A. A. *An Investigation of Liquefying Hybrid Rocket Fuels with Applications to Solar System Exploration*. *Ph.D. Thesis,* Stanford University, *2012.*

[6] Mehta, R. D. and Bradshaw, P., *Design Rules for Small Low Speed Wind Tunnels*, Aero. Journal (Royal Aeronautical Society), Vol. 73, 1979, pp. 443.

[7] Linstrom, P. and Mallard, W., NIST Chemistry WebBook, NIST Standard Reference Database, No. 69, Gaithersburg MD, December 2010.

[8] McBride, B. and Gordon, S., *Computer Program for Complex Chemical Equilibrium Compositions and Applications*, RP 1311, NASA, 1996.

[9] Karabeyoglu, A., Zilliac, G., Cantwell, B.J., DeZilwa, S. and Castellucci, P. *Scale-Up Tests of High Regression Rate Paraffin-Based Hybrid Rocket Fuels.* J of Prop and Power, Vol. 20, No. 6, November–December 2004.

[10] Haapanen, S., *Linear Stability Analysis and Direct Numerical Simulation of a Miscible Two-Fluid Channel Flow*, Ph.D. thesis, Stanford University, Stanford, CA, May 2008.